Experimental determination of the growth rate of Richtmyer-Meshkov induced turbulent mixing after reshock

G. Bouzgarrou[1], Y. Bury[1], S. Jamme[1], L. Joly[1], and J.-F. Haas[2]

1 Introduction

The Richtmyer-Meshkov Instability (RMI) develops when a shock wave impulsively accelerates an initially perturbed interface between two gases of different density, promoting their mixing inside a delimited zone, hereafter denoted the mixing zone (MZ). This mixing is a key issue for inertial confinement fusion process. It also finds applications in many different scientific and engineering issues, e.g. in supernova explosion or supersonic combustion [1]. In the context of inertial confinement fusion, the characterization of the RMI-induced mixing zone initiated by a shock and further amplified by a reshock is largely based on the temporal evolution of integral parameters such as the width of the MZ. This is classically achieved through shock tube experiments involving the time-resolved acquisition of Schlieren images. From the initial shock/interface interaction, the global evolution of the MZ growth rate is found to experience a succession of five consecutive phases: 1) linear increase, 2) asymptotic increase, 3) strong decrease (recompression of the MZ induced by the reshock), 4) linear increase, 5) asymptotic increase.

Among the various studies focusing on this topic [2, 3], recent works have explored the dynamics of a RMI-initiated MZ with a reshock. In their study about the growth rate evolution of the mixing zone consecutive to a reshock [4], Leinov and co-authors report that the post reshock growth rate, corresponding to the fourth phase, is largely independent of pre reshock conditions. These results differ from those obtained by Counilh *et al.* [5], where the mixing width after reshock is found to depend on pre reshock conditions. Since these various results were obtained via different post processing strategies of Schlieren images, one can thus question the relevance of a specific post processing methodology in the determination of the mixing dynamics.

[1] *Université de Toulouse, ISAE, 10 Avenue Edouard Belin, F-31055 Toulouse, France* · [2] *CEA, DAM, DIF, F-91297 Arpajon, France*

In an attempt to unravel this question, we propose to analyze a given set of shock tube experiments using various image processing algorithms in order to analyse the behaviour of the MZ growth rate after reshock.

2 Experimental set-up

The experimental apparatus used in this study consists of a 5m long, 130mm square cross section vertical shock tube. A schematic of the experimental setup is given in figure 1(a). An incident Mach 1.2 shock wave is generated by impacting a Mylar diaphragm, initially separating the driven and the driver sections of the shock tube, using a blade cutting device. The shock wave travels upward and crosses an air/sulphur hexafluoride (SF6) interface, which sets the Atwood number at 0.67. Both gases are initially separated by a thin nitrocellulosic membrane (0.5μm thick) trapped between two square-meshed grids. The lower grid ensures the mechanical resistance of the membrane under hydrostatic pressure of the heavy gas. The upper grid imposes a three-dimensional initial perturbation of wavelength equal to its mesh size. Pressure histories of the flow in the shock tube are obtained using five piezoelectric pressure transducers. The acquisition frequency is fixed to 2.5 MHz. The incident Mach number is determined via the two pressure transducers PPT1 and PPT2, located at 315 and 115mm below the interface respectively. In the test section, two additional pressure transducers PPT3 and PPT4 are flush-mounted at 43 and 213mm above the interface respectively. A fifth pressure transducer PPT5 is flush-mounted on the endwall of the test section. Time-resolved Schlieren visualizations are recorded thanks to a high-speed Phantom V12 camera. The data rate of the image recording is fixed to 27000 images per second with a spatial resolution equal to 512×384 pixels^2.

Several configurations are considered in order to analyze the interaction of a reshock with a MZ at different stages of its development (see $(X-t)$ diagram on figure 1(b)). To this avail two parameters, driving the spatio temporal evolution of the MZ, are considered: the length of the test section, hereafter denoted L, which fixes the arrival time of the reshock on the travelling mixing zone, and the wavelength of the initial perturbation (imposed by the upper grid mesh size), hereafter denoted λ. For convenience of reference, each experiment is referenced as C_L^λ, based on the values of L and λ. As such a first set of experiments $C_L^{1.8}$ is conducted, where L is varied from 100 to 300mm, in steps of 50mm, for an upper grid mesh size of $\lambda = 1.8$mm. This set of experiments is complemented with a second serie of experiments $C_L^{12.1}$, for which a $\lambda = 12.1$mm initial perturbation is considered for $L = 250$mm and $L = 300$mm. The temporal evolution of the MZ width, before and after its interaction with the reshock, is investigated through the analysis of post-processed Schlieren images, following specific filtering algorithms detailed in the next section.

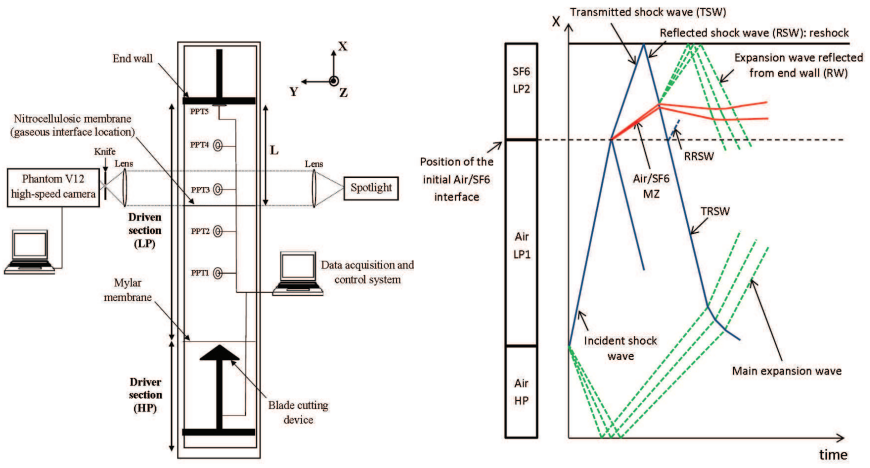

(a) (b)

Fig. 1 Description of the experimental apparatus (a) and (X-t) diagram of the experiment (b). Letters W, T and R used in the acronyms refer to 'wave', 'transmitted' and 'reflected' respectively.

3 Image processing methodology

Two distinct image post-processing algorithms have been developped in order to detect the MZ boundaries, based on spatial or frequential filtering techniques respectively. The spatial-based filtering approach decomposes into first, a median-filtering of the raw images, second an Otsu binarization and last an edge-based segmentation method (Canny filter) displaying the boundaries of the MZ. The frequency-based filtering approach consists in first, applying a 2D Fast Fourier Transform (FFT) on the raw images, second high-pass filtering the previously transformed images in order to eliminate the low frequency components of the image associated with the homogeneous zones, last applying the inverse FFT, revealing the boundaries of the MZ.

Once the boundaries of the MZ have been revealed by these two approaches, a region of interest (ROI) is then selected around the MZ inside each image, near the center of the tube in order to get rid of wall effects. For each column of the ROI, two pixels can be found as the boundaries, one on each side of the MZ. Therefore, the local width of the MZ in each column is obtained by subtracting the $X-$coordinate of these two pixels. The overall width of the MZ is finally determined by averaging all the widths of the MZ obtained in all the columns of the ROI.

As an illustration figure 2 shows the boundaries of the mixing zone as detected by the spatial and frequential filters respectively, before and after reshock. It has to be noticed that the spatial filter is found to be more sensitive to the transient presence, near the MZ, of spurious waves or membrane fragments that limit its efficiency in retrieving continuous boundaries on the whole history of the phenomenon (not illustrated here).

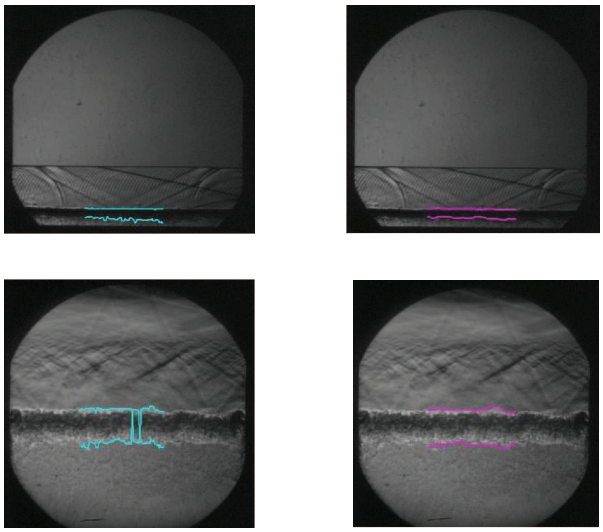

(a) (b)

Fig. 2 Schlieren images of the MZ at different instants for $L = 250$mm. Colored lines illustrate the boundaries obtained from (a) spatial algorithm, (b) frequential algorithm. Upper line: before reshock; lower line: after reshock.

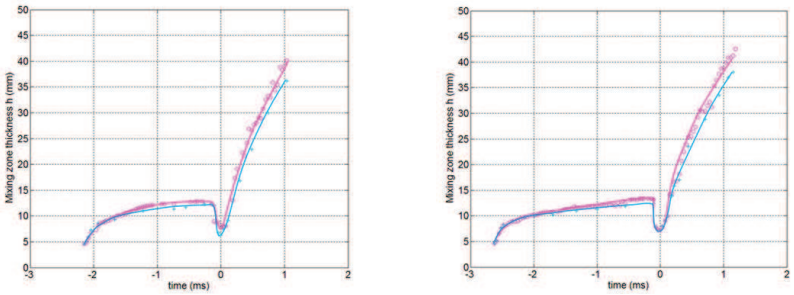

(a) (b)

Fig. 3 Temporal evolution of the MZ width obtained with spatial ($-*-$) and frequential ($-\circ-$) filters for $\lambda = 1.8$mm. (a) $L = 250$mm, (b) $L = 300$mm. Symbols: measurements. Solid lines: tendency curves.

Figure 3 presents the temporal evolution of the MZ width for cases $C_{250}^{1.8}$ and $C_{300}^{1.8}$. It shows that analogous evolutions of the MZ thickness are obtained from both spatial and frequential post processing algorithms. Similar growth rate evolutions are also observed when applying these two approaches for all the other considered cases. However, due to the previously mentioned robustness issues of the spatial filter, the latter provides a limited number of measurement points in comparison with the frequential one. As such and for sake of conciseness the analysis will thus hereafter be limited to the frequential filter.

4 Results and discussion

Figure 4 illustrates the topology of the MZ before its interaction with the reshock, for $L = 300$mm and for $\lambda = 1.8$mm (a) and $\lambda = 12.1$mm (b). Figure 5 summarizes the temporal evolution of the MZ width for experiments $C_L^{1.8}$ and $C_L^{12.1}$.

Figure 4 clearly shows that the global shape of the MZ is affected by the wavelength of the initial perturbation. Indeed, just before reshock and contrary to the case $C_{300}^{1.8}$, the MZ that develops in case $C_{300}^{12.1}$ depicts large corrugations on its upper boundary and spikes on its lower boundary. This emphasizes the influence of the wavelength of the initial perturbation on the topology of the MZ.

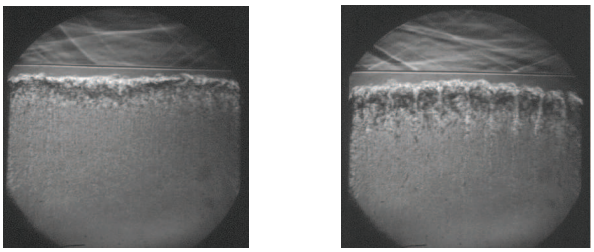

(a) (b)

Fig. 4 Schlieren images of the MZ just before reshock for $L = 300$mm. (a) $\lambda = 1.8$mm, (b) $\lambda = 12.1$mm.

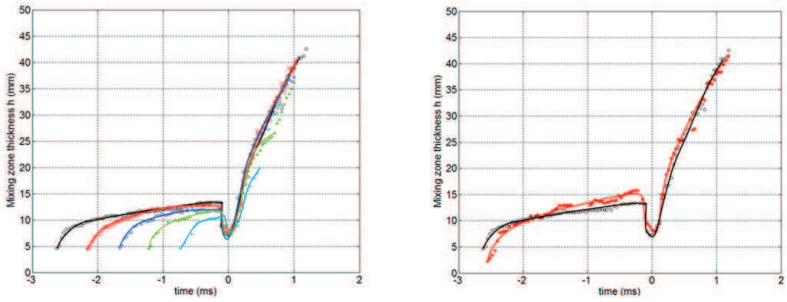

(a) (b)

Fig. 5 Temporal evolution of the MZ width obtained with the frequential filter for (a) $\lambda = 1.8$mm, $L = -\triangleright-$ 100, $-\triangle-$ 150, $-\diamond-$ 200, $-\square-$ 250 and $-\circ-$ 300mm ; (b) L =300mm, $-\square-$ $\lambda = 1.8$mm, $-\blacksquare-$ $\lambda = 12.1$mm. Symbols: measurements. Solid lines: tendency curves interrupted at the time of the interaction between the reshocked MZ and RW.

As expected, the analysis of figure 5(a) reveals that the temporal evolution of the MZ width, obtained before reshock for the different values of L considered in cases $C_L^{1.8}$, obeys a similar assymptotic trend until the MZ interacts with the reshock. Indeed as L is increased, the reshock occurs at different development times of the MZ,

imposing a greater or lesser MZ width at the time of reshock, comprised between $h = 10$mm for $L = 100$mm and $h = 14$mm for $L = 300$mm. In addition the influence of the wavelength of the initial perturbation ($\lambda = 1.8$mm *v.s.* $\lambda = 12.1$mm for $L = 300$mm), illustrated in figure 5(b) imposes slightly different assymptotic laws of the MZ width temporal evolution, leading to a larger MZ at the time of reshock when the wavelength is larger. Moreover and as previously evoked, the global topology of the MZ in case $C_{300}^{12.1}$ is also quite different from the case $C_{300}^{1.8}$.

Despite those differences it is remarkable to note that, independently of either the development state of the MZ (figure 5(a)) or the wavelength of the initial perturbation (figure 5(b)), the reshock causes the compression of the MZ to a fairly unique width of $h = 7$mm.

After the reshock, the evolution of the MZ width fits a similar trend for all the cases $C_L^{1.8}$ and $C_L^{12.1}$. It initially experiences a linear growth rate, between $t = 0$ms and $t = 0.15$ms, characterized by a slope close to $dh/dt \approx 21\mathrm{m/s}$. It should be noticed that this value is in good accordance with the empirical law defined by [6]. The post reshock evolution of the width of the MZ thus appears to be only weakly, if not, affected by its prior-to-reshock history. For subsequent instants the growth rate tends to decrease. However it is no more possible to determine a meaningful assymptotic analytical law since the expansion waves reflected from the endwall, referred to as RW on the $(X-t)$ diagram (figure 1(b)), quickly interacts with the reshocked MZ (about 1ms after the reshock for $L = 300$mm).

Acknowledgments

This work is supported by CEA, DAM, DIF under grant number 09-37-C-SACO.

References

1. Brouillette M. : The Richtmyer-Meshkov instability. Annu. Rev. Fluid Mech. **34**, pp. 445-468 (2002)
2. Vetter M., Sturtevant B. : Experiments on the Richtmyer-Meshkov instability of an air/SF6 interface. Shock Waves. **4**, pp. 247-252 (1995)
3. Erez L., Sadot O., Oron D., Erez G., Levin L.A., Shvarts D., Ben Dor G. : Study of the membrane effect on turbulent mixing measurements in shock tubes. Shock Waves. **10**, pp. 241-251 (2000)
4. Leinov E., Malamudi G., Elbaz Y., Levin L., Ben-Dor G., Shvarts D. and Sadot O. : Experimental and numerical investigation of the Richtmyer-Meshkov instability under re-shock conditions. J. Fluid Mech. **626**, pp. 449-475 (2009)
5. Counlih, D., Haas, J.F., Schwaederlé, L. : Measurements of turbulent mixing within an air/SF6 shocked and re-shocked interface. In 10th International Workshop on the Physics of Compressible Turbulent Mixing, Paris, France (2006)
6. Mikaelian K.O. : Turbulent mixing generated by Rayleigh-Taylor and Richtmyer-Meshkov instabilities. Physica D. **36**, pp. 343-57 (1989)